Cell Reports
Report

Structure and Mechanism of a Nitrate Transporter

Hanchi Yan,[1,3,4] Weiyun Huang,[1,3,4] Chuangye Yan,[1,3] Xinqi Gong,[1,3] Sirui Jiang,[1,3] Yu Zhao,[1,3] Jiawei Wang,[2,3] and Yigong Shi[1,3,*]
[1]Ministry of Education Key Laboratory of Protein Science
[2]State Key Laboratory of Bio-membrane and Membrane Biotechnology
[3]Tsinghua-Peking Joint Center for Life Sciences, Center for Structural Biology, School of Life Sciences and School of Medicine Tsinghua University, Beijing 100084, China
[4]These authors contributed equally to this work
*Correspondence: shi-lab@tsinghua.edu.cn
http://dx.doi.org/10.1016/j.celrep.2013.03.007

SUMMARY

The nitrate/nitrite transporters NarK and NarU play an important role in nitrogen homeostasis in bacteria and belong to the nitrate/nitrite porter family (NNP) of the major facilitator superfamily (MFS) fold. The structure and functional mechanism of NarK and NarU remain unknown. Here, we report the crystal structure of NarU at a resolution of 3.1 Å and systematic biochemical characterization. The two molecules of NarU in an asymmetric unit exhibit two distinct conformational states: occluded and partially inward-open. The substrate molecule nitrate appears to be coordinated by four highly conserved, charged, or polar amino acids. Structural and biochemical analyses allowed the identification of key amino acids that are involved in substrate gating and transport. The observed conformational differences of NarU, together with unique sequence features of the NNP family transporters, suggest a transport mechanism that might deviate from the canonical rocker-switch model.

INTRODUCTION

Gaseous nitrogen is unfit for biological utilization by most organisms except diazotrophs, which can fix and consume atmospheric nitrogen. Environmental nitrogen is supplied to microbes and plants mainly in the forms of nitrate (NO_3^-), nitrite (NO_2^-), and ammonium (NH_4^+). Nitrate and nitrite must be reduced for conversion to ammonium, which then can be used for synthesis of amino acids and regulation of other biological pathways.

Uptake of nitrogen oxyanion (nitrate and nitrite) is mediated by nitrate/nitrite transporters, of which a major fraction constitute the nitrate/nitrite porter (NNP) family within the major facilitator superfamily (MFS) (Jia and Cole, 2005; Moir and Wood, 2001; Pao et al., 1998). NNPs include the bacterial NarK family, exemplified by NarK and NarU in *E. coli* (Jia and Cole, 2005; Moir and Wood, 2001), and the plant NRT2 high-affinity nitrate transporters (Orsel et al., 2002; Tsay et al., 2007). NarK and NarU share 76% sequence identity and transport both nitrate and nitrite (Clegg et al., 2002; Clegg et al., 2006; Jia et al., 2009). NarU plays a key role during severe nutrient starvation (Clegg et al., 2006). NRT2.1 participates in the lateral root initiation and regulates root plasticity (Little et al., 2005; Remans et al., 2006). NRT2.4 is essential for nitrate uptake in plant roots and shoots under conditions of low nitrate supply (Kiba et al., 2012).

The sequence identity between prokaryotic and eukaryotic NNP members is only 14%–18%. All NNP transporters, including NarK and NarU, share two conserved glycine-rich nitrate signature motifs (Trueman et al., 1996; Unkles et al., 2012; Unkles et al., 2004). These characteristic motifs, not found in any other transporter of the MFS fold, relate to substrate specificity and transport mechanism (Trueman et al., 1996; Unkles et al., 2012; Unkles et al., 2004). In addition, two highly conserved Arg residues, corresponding to Arg87 and Arg303 in NarU, are required for substrate binding in the eukaryotic NNP family transporter NrtA (Unkles et al., 2004).

The transport mechanism of NarK and NarU remains largely enigmatic. Investigation of the nitrate transport mechanism is hampered by the technical difficulty of finding a suitable radioisotopic substrate. To date, it remains unclear whether NarK is a nitrate-nitrite antiporter or a symporter (Boogerd et al., 1983; Jia and Cole, 2005; Moir and Wood, 2001). Understanding the transport mechanism is further confounded by a lack of structural information on NarK or NarU.

RESULTS

Functional Characterization of NarU

The recombinant full-length NarU (residues 1–462) binds to nitrate with a dissociation constant of approximately 33.7 μM (Table S1). Compared to nitrate, the binding affinity for nitrite is about 10-fold lower (Table S1). Notably, the binding reactions are endothermic, as determined by isothermal titration calorimetry (ITC, Figures 1A and 1B).

Reconstitution of an in vitro transport assay for nitrate or nitrite has been extremely challenging, because the longest half-life for radioactive nitrogen or oxygen is only about 10 min for ^{13}N or 2 min for ^{15}O. To circumvent this problem, we built an indirect stopped-flow assay (Figure 1C), in which liposomes were quickly mixed with various solutes. Upon mixing with 50 mM nitrate or other solutes, water efflux through the lipid bilayer caused the protein-free liposomes to rapidly deflate, resulting in a sharp increase of the light scattering signal. The deflated liposomes remained unchanged over

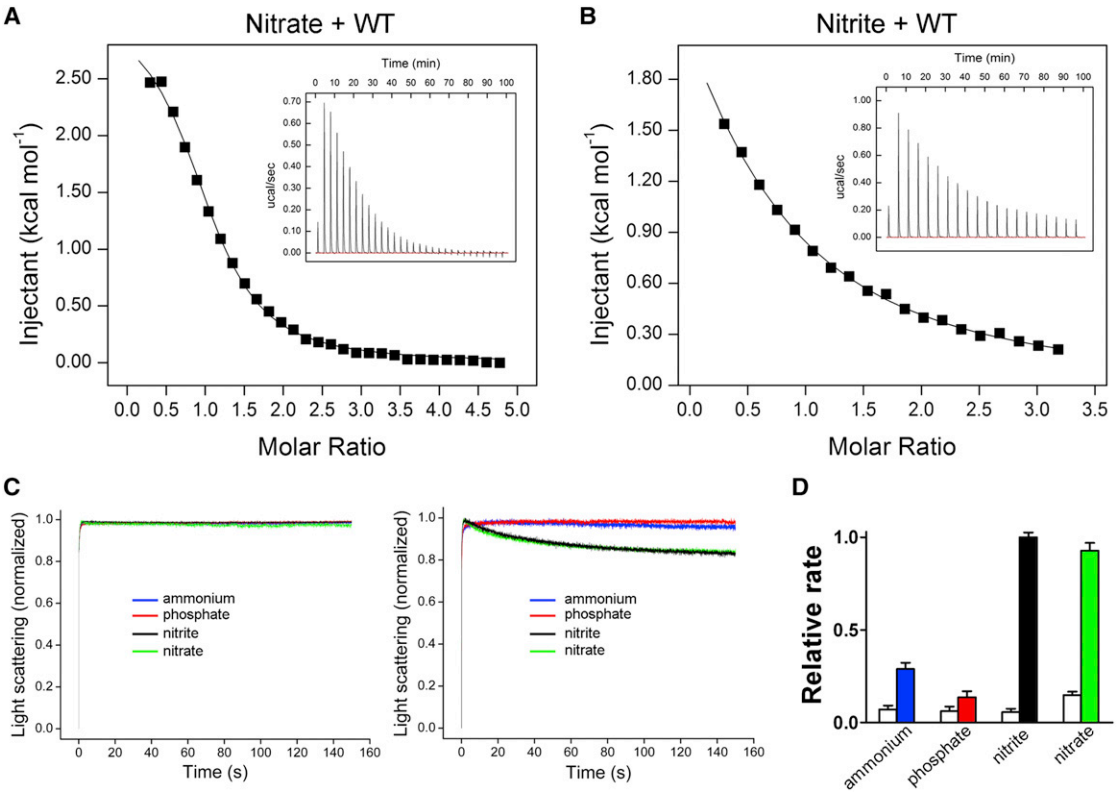

Figure 1. Functional Characterization of NarU

(A) Nitrate binding by wild-type (WT) NarU as measured by isothermal titration calorimetry (ITC). The binding affinity between nitrate and WT NarU was estimated to be ~33 μM.

(B) Measurement of binding affinity between nitrite and WT NarU. The binding affinity for nitrite is ~373 μM, or ~10-fold lower than that for nitrate.

(C) NarU exhibits transport specificity for nitrate and nitrite. Substrate transport was measured by the stopped-flow assay. The left panel shows the control, where light scattering was measured on NarU-free liposomes. The right panel shows the results with NarU-incorporated proteoliposomes.

(D) Quantification of experimental results in (C). The white bars indicate the controls.

All error bars represent the SD of three independent experiments.

See also Table S1.

a time frame of 150 s (Figure 1C, left panel). Mixing with nitrate also caused the NarU-incorporated proteoliposomes to deflate similarly to the protein-free liposomes; however, the proteoliposomes reswell over time, as judged by the decreasing signal of light scattering (Figure 1C, right panel, green line). The reswelling is most likely due to NarU-mediated nitrate transport, which decreases the osmotic pressure across the lipid bilayer. The reswelling was observed for nitrite, but not for phosphate or ammonium (Figure 1C, right panel). Curve fitting revealed that NarU transports nitrate and nitrite at similar rates (Figure 1D). The substrate specificity is manifested by the much reduced rates of transport for phosphate or ammonium as compared to nitrate or nitrite.

Structure of NarU

Native NarU was crystallized in the absence of substrate in the space group $P2_12_12_1$, with two molecules in each asymmetric unit. Selenomethionine-substituted NarU was similarly crystallized in the presence of 5 mM nitrate. The structure of NarU was determined at a resolution of 3.1 Å with the use of selenium-based single-wavelength anomalous dispersion (Table S2 and Figure S1). The experimental electron density is of sufficient quality for model building, which was facilitated by the 26 selenium peaks in each asymmetric unit (Figures S1A and S1B). The final atomic model agrees well with the calculated 2Fo-Fc map (Figures S1C–S1F). The structure of native NarU in the absence of substrate was determined by molecular replacement (Table S2).

Similar to other MFS transporters (Abramson et al., 2003; Huang et al., 2003), NarU comprises 12 transmembranes (TMs), TMs 1–6 and 7–12 being the N-terminal and C-terminal domains, respectively (Figure 2A). These two domains are related by a pseudo 2-fold axis that is parallel to the membrane normal. Each domain contains a pair of inverted repeats, TMs 1–3 and 4–6 in the N-terminal domain and TMs 7–9 and 10–12 in the C-terminal domain (Figure S1I). The inverted repeats within each domain are related by a 2-fold axis perpendicular to the membrane normal. The membrane-embedded surface of NarU is hydrophobic, with the cytoplasmic boundary demarcated by positive electrostatic potential (Figure 2B).

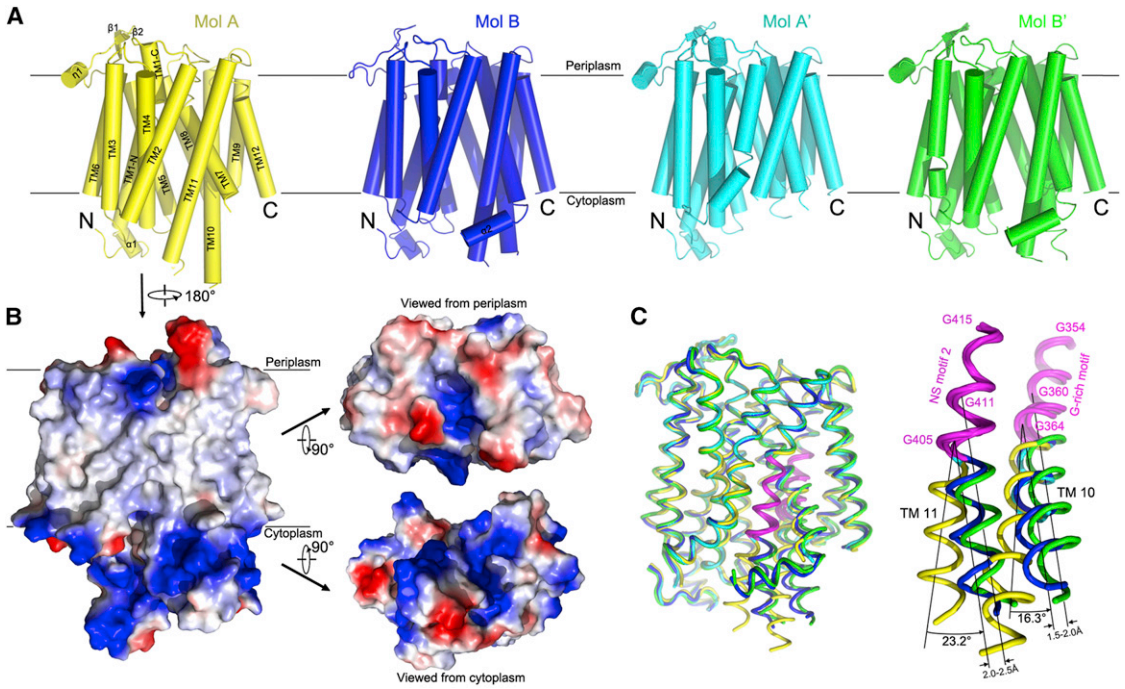

Figure 2. Overall Structure of NarU

(A) Structure of NarU in two distinct conformations. There are two NarU molecules in an asymmetric unit. Mol A (color yellow) adopts an occluded conformation, and Mol B (blue) and Mol B' (green) have a partially inward-open conformation. Each NarU molecule consists of 12 transmembrane (TM) helices.

(B) The surface electrostatic potential of NarU. The membrane-spanning portion is hydrophobic, and the periplasmic and cytoplasmic sides of NarU are enriched by hydrophilic and charged amino acids.

(C) A structural overlay of NarU molecules reveals structural shifts in TM10 and TM11. The C-terminal half of TM10 and the N-terminal half of TM11 in Mol B are bent by 16° and 23°, respectively, relative to Mol A. All structure images in this paper were produced with PyMOL (DeLano, 2002).

See also Table S2 and Figures S1 and S3.

The two molecules of NarU crystallized in the presence of nitrate (Mol A and Mol B) exhibit different conformations: Mol A and Mol B correspond to Mol A' and Mol B', respectively, of native NarU crystallized in the absence of nitrate (Figure 2A). Mol A adopts an occluded conformation, whereas Mol B and Mol B' partially open to the cytoplasmic side. Portions of TM10 and TM11 in Mol A' have poor electron density, precluding judgment about its conformational state. Comparison of these four molecules revealed few overall structural changes. Mol A and Mol B have a root-mean-square deviation (rmsd) of approximately 0.55 Å over 314 aligned Cα atoms. However, TM10 and TM11 exhibit obvious structural differences in these four NarU molecules (Figure 2C). As compared to the occluded conformation (Mol A), the C-terminal half of TM10 and the N-terminal half of TM11 in Mol B rotate approximately 16° and 23°, respectively, around Gly364 and Gly405, to move away from the center toward the periphery.

Putative Substrate-Binding Site

Two positively charged amino acids, Arg87 and Arg303, and two polar residues, Asn173 and Tyr261, are buried at the center of Mol A (Figure 3A and Figure S2A). These four amino acids exhibit well-defined electron density (Figure S2A) and are invariant among NarU and its sequence homologs (Figure S3), suggesting functional importance. Supporting this analysis, Arg87 and Arg303 were found to be essential for the transport activity of NarU in *E. coli* (Jia and Cole, 2005; Jia et al., 2009). The corresponding Arg residues in the eukaryotic NNP family transporter NrtA are required for nitrate binding and transport (Unkles et al., 2004). A patch of electron density is located at the center of these four amino acids (Figure 3A and Figure S2A). Importantly, the electron density depends on inclusion of 5 mM nitrate in the crystallization buffer, given that removal of nitrate from the crystallization buffer led to drastically weakened electron density for the four amino acids and their vicinity (Figure S2B). This analysis suggests that the electron density may come from nitrate. Modeling of nitrate into the electron density allows the formation of six hydrogen bonds (H-bonds) with the four surrounding amino acids (Figure 3A). There is no clear electron density at the substrate-binding site of Mol B; hence, no substrate was modeled at the site.

To further investigate the functional role, we individually mutated these four amino acids to Ala and measured the mutants' binding affinities toward nitrate and nitrite (Figures S4A and S4C). Three NarU mutants, R87A, R303A, and Y261A, completely abrogated binding to nitrate or nitrite. NarU-N173A retained some binding to substrate, albeit drastically reduced in comparison to wild-type (WT) NarU; the binding affinities could not be reliably estimated. Next, we examined the impact of these mutations on the transport activity of NarU. In comparison to WT

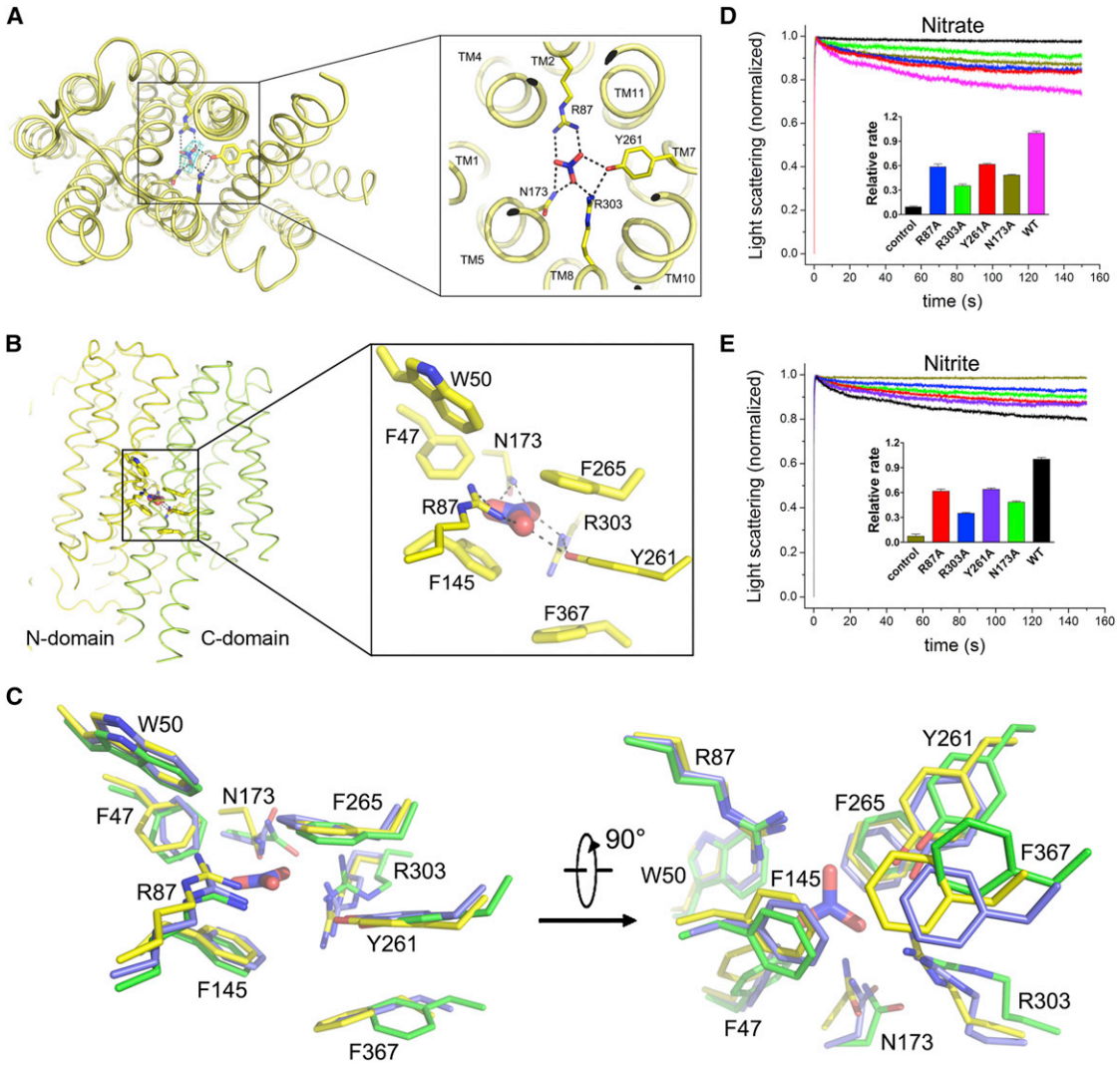

Figure 3. Identification and Features of the Substrate-Binding Site

(A) Identification of a putative substrate-binding site. The Fo-Fc electron density, contoured at 2.5σ and located at the center of the NarU molecule, is surrounded by four conserved amino acids, suggesting a substrate-binding site (left panel). A close-up view shows two positively charged amino acids, Arg87 and Arg303, and two polar residues, Asn173 and Tyr261 (right panel).

(B) Features of the substrate-binding-site sandwich. The charged and polar binding residues for substrate are sandwiched between two layers of hydrophobic amino acids. The close-up image in the right panel highlights the key residues.

(C) A close-up comparison of the substrate-binding-site residues in molecules A (yellow), B (blue), and B' (green). These residues are mostly superimposable, with noticeable changes on the position of Phe367.

(D and E) Characterization of the transport activity for WT and mutant NarU. Compared to WT NarU, the missense mutants R87A, R303A, Y271A, and N173A show lower permeability for nitrate and nitrite.

All error bars represent the SD of three independent experiments.

See also Table S1 and Figures S2, S3, and S4.

NarU, the relative rate of transport for nitrate and nitrite was decreased between 40% and 60%, but not abrogated, for each of the four NarU missense mutants (Figures 3D and 3E).

The charged, polar substrate-binding site is sandwiched between two layers of hydrophobic amino acids (Figures 3B and 3C). The hydrophobic layer toward the periplasmic side comprises Phe47, Trp50, and Phe265, whereas the cytoplasmic layer comprises Phe145 and Phe367. Of the five residues, Phe47, Phe145, and Phe367 are invariant among all NarU homologs in bacteria and eukaryotes (Figure S3). The NarU mutants F47A, W50A, and F367A abrogated binding to both nitrate and nitrite, and F265A retained very weak binding to nitrate but not to nitrite (Figures S4B and S4D). Only F145A displayed binding to both nitrate and nitrite. It should be noted that, although most residues at the substrate-binding site are largely superimposable among molecules A, B, and B', Phe367 displays noticeable changes, suggesting a role in substrate upload or release (Figure 3C).

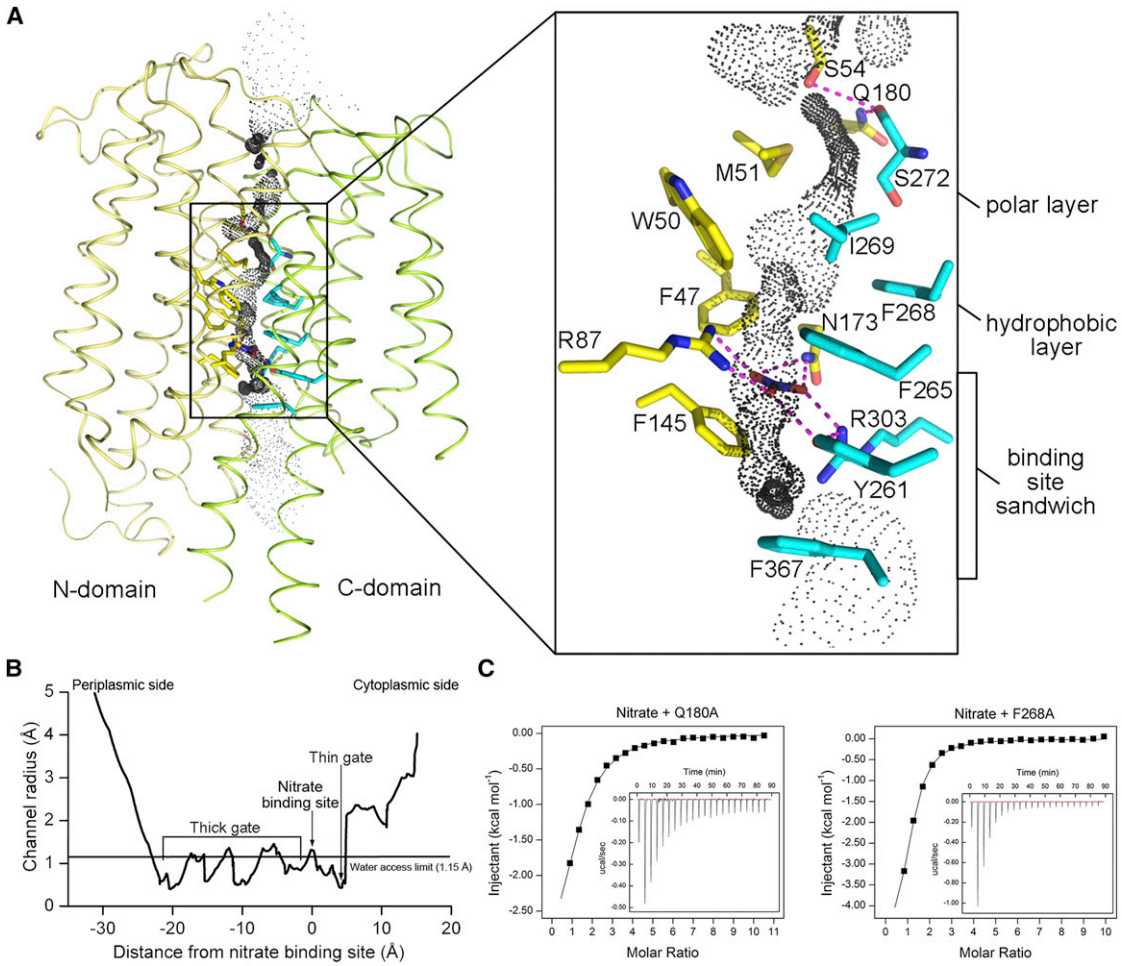

Figure 4. Structural Features of the NarU Transport Path

(A) The transport path between N-terminal and C-terminal domains contains a thin gate and a thick gate. The thin gate on the cytoplasmic side consists of only Phe145 and Phe367. The thick gate on the periplasmic side has two hydrophobic layers, one comprising Phe47, Trp50, and Phe265 and the other comprising Met51, Phe268, Ile269, as well as a polar layer comprising Ser54, Gln180, Ser272.

(B) Radii of the NarU transport path in Mol A, calculated by HOLE (Smart et al., 1993).

(C) Impact of mutation in the thick gate on substrate binding. Shown here are the ITC results for the NarU mutants Q180A and F268A. The binding reactions have turned from endothermic for WT NarU to exothermic for mutant NarU.

See also Table S1 and Figures S3 and S5.

Transport Path

The MFS-fold proteins are thought to transport substrate through an axial path between the N-terminal and C-terminal domains (Figures 4A and 4B) (Law et al., 2008). The putative substrate-binding site is insulated from the cytoplasmic side by only two conserved amino acids, Phe145 and Phe367, which most likely constitute the thin gate (Krishnamurthy et al., 2009). The exit of nitrate to the periplasm is blocked by a number of potential gating residues (Figure 4A), of which three amino acids, Ser54, Gln180, and Ser272, constitute an interacting polar layer, and Met51, Phe268, Ile269 form an additional hydrophobic layer between the polar layer and the binding-site sandwich. The hydrophobic residues (Met51, Phe268, Ile269, Phe47, Trp50, and Phe265) in the two hydrophobic layers mediate extensive van der Waals contacts, which help maintain the outward-closed conformation of NarU. The polar layer and the two hydrophobic layers together may constitute the thick gate (Krishnamurthy et al., 2009).

We speculated that disruption of the observed interactions in NarU might lead to altered substrate binding. We generated four NarU mutants, each involving a missense mutation of a putative gating residue to Ala, and assessed their binding to nitrate and nitrite. In sharp contrast to WT NarU, most of the binding reactions for these mutants are exothermic (Figure 4C and Figures S5A–S5C). The only exception is the mutant S272A, which still exhibits endothermic binding. Structurally, the S272A mutation may be silent, because only the main chain of Ser272 is involved in the gating interactions.

The substrate entry region on the periplasmic side contains three positively charged amino acids: Lys62, Lys280, and

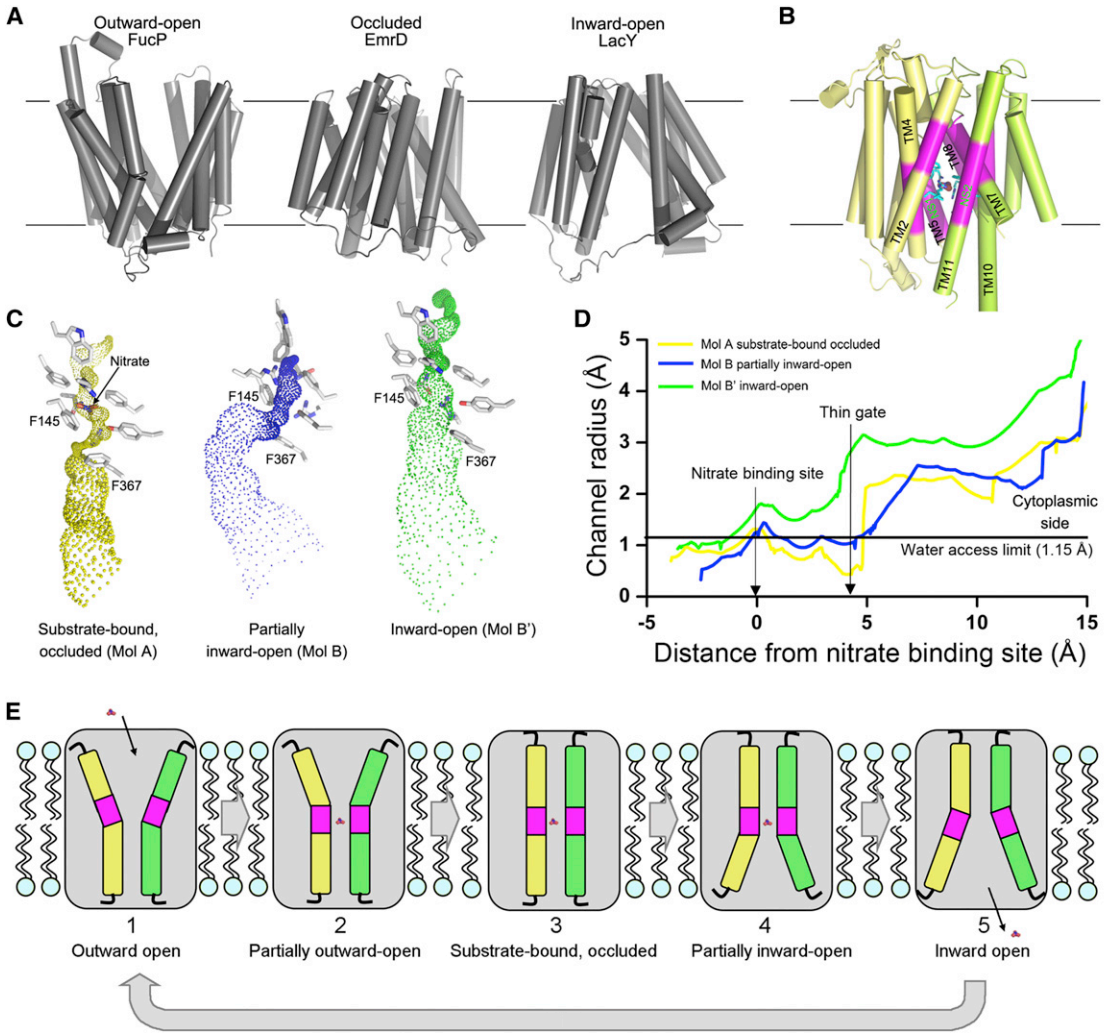

Figure 5. A Working Model for NarU and Other NNP Family Transporters

(A) Three essential conformational states of MFS transporters. Shown here are the structures of outward-open FucP (PDB code 3O7Q), occluded EmrD (PDB code 2GFP), and inward-open LacY (PDB code 1PV7). Alternating access is thought to be achieved by the rocker-switch model, involving these three conformations for the MFS.

(B) The substrate-binding site is surrounded by Gly-rich sequences in TM4, TM5, TM7, TM8, TM10, and TM11 (colored magenta).

(C) Molecules B and B' exhibit different inward-open degrees. Shown here are the calculated surfaces of molecules A, B, and B', from the cytoplasmic side to the substrate-binding site, calculated by HOLE (Smart et al., 1993).

(D) Calculated radii of the NarU transport path in molecules A, B, and B'.

(E) A proposed model of conformational changes for the NNP family transporters. We suggest that, in contrast to the rocker-switch model, the overall relative orientation of the N-terminal and C-terminal domains remain largely unchanged during substrate transport. Substrate binding and release are accompanied mainly by bending of groups of TMs, which is facilitated by the Gly-rich sequences.

See also Figure S3.

Arg290 (Figure S3). It is possible that these residues may play a role in recruitment of the negatively charged substrate. To examine this possibility, we generated two missense mutants: K62A and R290A. Neither mutation has a pronounced effect on substrate binding affinity (Figures S5B and S5D; Table S1), because the affected amino acids are far away from the putative substrate-binding site. However, both mutants exhibit greatly diminished transport activity in comparison to WT NarU (Figures S5E and 5F; Table S1).

Implication for Transport Mechanism

The transport mechanism for the MFS transporters is believed to follow the rocker-switch model (Forrest et al., 2011; Law et al., 2008), in which alternating access to periplasm and cytoplasm is achieved by a rigid-body rotation of the N-terminal domain relative to the C-terminal domain. This model predicts three essential conformations: outward-open, occluded, and inward-open (Figure 5A). The rocker-switch model is generally supported by structural analyses of the MFS transporters, which

nonetheless have revealed at least five distinct conformations: the inward-open LacY (Abramson et al., 2003; Guan et al., 2007; Mirza et al., 2006) and GlpT (Huang et al., 2003), the occluded EmrD (Yin et al., 2006), the outward-open FucP (Dang et al., 2010), the outward-facing, partially occluded XylE (Sun et al., 2012), and the inward-occluded $PepT_{So}$ (Newstead et al., 2011) and $PepT_{St}$ (Solcan et al., 2012). Comparison of these structures reveals few structural differences among the N-terminal domains or C-terminal domains, consistent with the rigid-body movement required for the rocker-switch model (Law et al., 2008).

What distinguishes the NNP family transporters from other MFS proteins is the presence of Gly-rich nitrate signature motifs in TM5 and TM11. In addition, conserved Gly residues are also present in TM4, TM7, TM8, and TM10 (Figure S3). Strikingly, these Gly-rich sequences constitute the inner core of the TMs, surrounding the putative substrate-binding site (Figure 5B). These Gly residues might allow a greater degree of conformational flexibility. Indeed, the only pronounced structural difference in NarU is the bending of TM10 and TM11 in Mol B relative to those in Mol A (Figure 2C and Movie S1). Mol B and Mol B' have different inward-open degrees yet identical domain organization (Figures 5C and 5D). This analysis suggests a model whereby bending of transmembrane helices within the N-terminal and C-terminal domains, rather than rigid-body movement of these two domains, might be associated with substrate transport (Figure 5E). This model is favored by the small size of nitrate, which has an ionic radius of only ~1.96 Å (Masterton et al., 1971). Nonetheless, we acknowledge the highly speculative nature of our model.

Perspective

Given the lack of radioisotope-labeled substrates with a long half-life, we qualitatively assessed the transport activity of NarU by using a liposome-based stopped-flow assay. Although this assay fails to yield absolute rates of substrate transport, it allows the comparison of relative transport rates by various NarU mutants and the assessment of relative transport rates for different substrates. It should be noted, however, that the relative transport rates for different substrates cannot be directly compared, because what was measured is not transport rate but the rate of water influx into the proteoliposomes.

Glycine residues in the nitrate signature motifs of NrtA are required for the flexibility of the TMs and are involved in the transport activity of NrtA (Unkles et al., 2012). This finding, supported by our structural analysis, is consistent with our proposed transport model. On the basis of GlpT and FucP, a structural model of NrtA in the outward-open and inward-open states was proposed (Unkles et al., 2012). Assignment of binding-site residues and overall arrangement of the TMs are generally consistent with the NarU structure, although detailed assessment has yet to be performed because of the lack of atomic coordinates for the NrtA models. The distance between the two Arg residues in NrtA was predicted to be 15 Å, whereas the measured distance is about 7–8 Å in the four NarU molecules. Finally, Asn459 in TM11 of NrtA is highly conserved in eukaryotic homologs of NarU and plays an important role in substrate transport (Unkles et al., 2012); however, this residue is not conserved in NarU and other bacterial homologs, suggesting some variation of substrate transport between prokaryotes and eukaryotes.

The fact that NarU-incorporated liposomes allowed water influx over time is inconsistent with the scenario of a nitrate-nitrite antiporter, because an obligatory nitrate-nitrite antiporter would be unable to reduce the osmotic pressure across the liposome bilayer. This analysis favors the possibility that NarU is most likely a symporter rather than an antiporter. Our experimental analysis revealed no detectable pH change for NarU after substrate transport (Figure S6A); by contrast, there was an obvious pH change for the known proton-coupled transporter NirC (Rycovska et al., 2012). Therefore, it is unlikely that NarU is an H^+-coupled transporter. Additional experiments suggest that NarU was able to transport nitrate under sodium salt only, potassium salt only, or both (Figure S6B). Under the limit of our experimental conditions, the result suggests the possibility that NarU might allow both the sodium and potassium ion as the co-transported cation.

EXPERIMENTAL PROCEDURES

The recombinant NarU protein was overexpressed in *E. coli* and purified to homogeneity. The purified NarU was crystallized by the hanging-drop vapor-diffusion method. All data sets were collected at the Shanghai Synchrotron Radiation Facility (SSRF), beamline BL17U, and processed with HKL2000 (Otwinowski and Minor, 1997) and the CCP4 suite (Collaborative Computational Project, Number 4, 1994). The experimental phase was generated by Se-SAD with SHELX (Schneider and Sheldrick, 2002) and improved by DM (Cowtan, 1994). The model was built by COOT (Emsley and Cowtan, 2004) and refined with PHENIX (Adams et al., 2002) and the CCP4 suite. Substrate binding affinity of NarU was measured by isothermal titration calorimetry (ITC). Liposome-based transport assay of NarU was performed as described previously (Fu et al., 2000; Wang et al., 2009). Molecular dynamics simulation on NarU was performed according to the published protocol (Lezon and Bahar, 2012).

See Extended Experimental Procedures for details.

ACCESSION NUMBERS

The atomic coordinates of NarU have been deposited in the Protein Data Bank under the accession codes 4IU8 and 4IU9.

SUPPLEMENTAL INFORMATION

Supplemental Information includes Extended Experimental Procedures, six figures, two tables, and one movie and can be found with this article online at http://dx.doi.org/10.1016/j.celrep.2013.03.007.

LICENSING INFORMATION

ACKNOWLEDGMENTS

This work was supported by the National Key Basic Research Program of China (2009CB918801 and 2013CB910602) and the National Natural Science Foundation of China (projects 31021002, 31130002, and 31170680).

Received: October 25, 2012
Revised: January 20, 2013
Accepted: March 6, 2013
Published: March 21, 2013

REFERENCES

Abramson, J., Smirnova, I., Kasho, V., Verner, G., Kaback, H.R., and Iwata, S. (2003). Structure and mechanism of the lactose permease of Escherichia coli. Science *301*, 610–615.

Adams, P.D., Grosse-Kunstleve, R.W., Hung, L.W., Ioerger, T.R., McCoy, A.J., Moriarty, N.W., Read, R.J., Sacchettini, J.C., Sauter, N.K., and Terwilliger, T.C. (2002). PHENIX: building new software for automated crystallographic structure determination. Acta Crystallogr. D Biol. Crystallogr. *58*, 1948–1954.

Boogerd, F.C., Van Verseveld, H.W., and Stouthamer, A.H. (1983). Dissimilatory nitrate uptake in Paracoccus denitrificans via a ΔμH-dependent system and a nitrate-nitrite antiport system. Biochim. Biophys. Acta *723*, 415–427.

Clegg, S., Yu, F., Griffiths, L., and Cole, J.A. (2002). The roles of the polytopic membrane proteins NarK, NarU and NirC in Escherichia coli K-12: two nitrate and three nitrite transporters. Mol. Microbiol. *44*, 143–155.

Clegg, S.J., Jia, W., and Cole, J.A. (2006). Role of the Escherichia coli nitrate transport protein, NarU, in survival during severe nutrient starvation and slow growth. Microbiology *152*, 2091–2100.

Collaborative Computational Project, Number 4. (1994). The CCP4 suite: programs for protein crystallography. Acta Crystallogr. D Biol. Crystallogr. *50*, 760–763.

Cowtan, K. (1994). DM: An automated procedure for phase improvement by density modification. Joint CCP4 and ESF-EACBM Newsletter on Protein Crystallography *31*, 34–38.

Dang, S., Sun, L., Huang, Y., Lu, F., Liu, Y., Gong, H., Wang, J., and Yan, N. (2010). Structure of a fucose transporter in an outward-open conformation. Nature *467*, 734–738.

DeLano, W.L. (2002). The PyMOL Molecular Graphics System. http://www.pymol.org.

Emsley, P., and Cowtan, K. (2004). Coot: model-building tools for molecular graphics. Acta Crystallogr. D Biol. Crystallogr. *60*, 2126–2132.

Forrest, L.R., Krämer, R., and Ziegler, C. (2011). The structural basis of secondary active transport mechanisms. Biochim. Biophys. Acta *1807*, 167–188.

Fu, D., Libson, A., Miercke, L.J., Weitzman, C., Nollert, P., Krucinski, J., and Stroud, R.M. (2000). Structure of a glycerol-conducting channel and the basis for its selectivity. Science *290*, 481–486.

Guan, L., Mirza, O., Verner, G., Iwata, S., and Kaback, H.R. (2007). Structural determination of wild-type lactose permease. Proc. Natl. Acad. Sci. USA *104*, 15294–15298.

Huang, Y., Lemieux, M.J., Song, J., Auer, M., and Wang, D.N. (2003). Structure and mechanism of the glycerol-3-phosphate transporter from Escherichia coli. Science *301*, 616–620.

Jia, W., and Cole, J.A. (2005). Nitrate and nitrite transport in Escherichia coli. Biochem. Soc. Trans. *33*, 159–161.

Jia, W., Tovell, N., Clegg, S., Trimmer, M., and Cole, J. (2009). A single channel for nitrate uptake, nitrite export and nitrite uptake by Escherichia coli NarU and a role for NirC in nitrite export and uptake. Biochem. J. *417*, 297–304.

Kiba, T., Feria-Bourrellier, A.B., Lafouge, F., Lezhneva, L., Boutet-Mercey, S., Orsel, M., Bréhaut, V., Miller, A., Daniel-Vedele, F., Sakakibara, H., and Krapp, A. (2012). The Arabidopsis nitrate transporter NRT2.4 plays a double role in roots and shoots of nitrogen-starved plants. Plant Cell *24*, 245–258.

Krishnamurthy, H., Piscitelli, C.L., and Gouaux, E. (2009). Unlocking the molecular secrets of sodium-coupled transporters. Nature *459*, 347–355.

Law, C.J., Maloney, P.C., and Wang, D.N. (2008). Ins and outs of major facilitator superfamily antiporters. Annu. Rev. Microbiol. *62*, 289–305.

Lezon, T.R., and Bahar, I. (2012). Constraints imposed by the membrane selectively guide the alternating access dynamics of the glutamate transporter GltPh. Biophys. J. *102*, 1331–1340.

Little, D.Y., Rao, H., Oliva, S., Daniel-Vedele, F., Krapp, A., and Malamy, J.E. (2005). The putative high-affinity nitrate transporter NRT2.1 represses lateral root initiation in response to nutritional cues. Proc. Natl. Acad. Sci. USA *102*, 13693–13698.

Masterton, W.L., Bolocofsky, D., and Lee, T.P. (1971). Ionic radii from scaled particle theory of the salt effect. J. Phys. Chem. *75*, 2809–2815.

Mirza, O., Guan, L., Verner, G., Iwata, S., and Kaback, H.R. (2006). Structural evidence for induced fit and a mechanism for sugar/H+ symport in LacY. EMBO J. *25*, 1177–1183.

Moir, J.W., and Wood, N.J. (2001). Nitrate and nitrite transport in bacteria. Cell. Mol. Life Sci. *58*, 215–224.

Newstead, S., Drew, D., Cameron, A.D., Postis, V.L., Xia, X., Fowler, P.W., Ingram, J.C., Carpenter, E.P., Sansom, M.S., McPherson, M.J., et al. (2011). Crystal structure of a prokaryotic homologue of the mammalian oligopeptide-proton symporters, PepT1 and PepT2. EMBO J. *30*, 417–426.

Orsel, M., Krapp, A., and Daniel-Vedele, F. (2002). Analysis of the NRT2 nitrate transporter family in Arabidopsis. Structure and gene expression. Plant Physiol. *129*, 886–896.

Otwinowski, Z., and Minor, W. (1997). Processing of X-ray diffraction data collected in oscillation mode. Methods Enzymol. *276*, 307–326.

Pao, S.S., Paulsen, I.T., and Saier, M.H., Jr. (1998). Major facilitator superfamily. Microbiol. Mol. Biol. Rev. *62*, 1–34.

Remans, T., Nacry, P., Pervent, M., Girin, T., Tillard, P., Lepetit, M., and Gojon, A. (2006). A central role for the nitrate transporter NRT2.1 in the integrated morphological and physiological responses of the root system to nitrogen limitation in Arabidopsis. Plant Physiol. *140*, 909–921.

Rycovska, A., Hatahet, L., Fendler, K., and Michel, H. (2012). The nitrite transport protein NirC from Salmonella typhimurium is a nitrite/proton antiporter. Biochim. Biophys. Acta *1818*, 1342–1350.

Schneider, T.R., and Sheldrick, G.M. (2002). Substructure solution with SHELXD. Acta Crystallogr. D Biol. Crystallogr. *58*, 1772–1779.

Smart, O.S., Goodfellow, J.M., and Wallace, B.A. (1993). The pore dimensions of gramicidin A. Biophys. J. *65*, 2455–2460.

Solcan, N., Kwok, J., Fowler, P.W., Cameron, A.D., Drew, D., Iwata, S., and Newstead, S. (2012). Alternating access mechanism in the POT family of oligopeptide transporters. EMBO J. *31*, 3411–3421.

Sun, L., Zeng, X., Yan, C., Sun, X., Gong, X., Rao, Y., and Yan, N. (2012). Crystal structure of a bacterial homologue of glucose transporters GLUT1-4. Nature *490*, 361–366.

Trueman, L.J., Richardson, A., and Forde, B.G. (1996). Molecular cloning of higher plant homologues of the high-affinity nitrate transporters of Chlamydomonas reinhardtii and Aspergillus nidulans. Gene *175*, 223–231.

Tsay, Y.F., Chiu, C.C., Tsai, C.B., Ho, C.H., and Hsu, P.K. (2007). Nitrate transporters and peptide transporters. FEBS Lett. *581*, 2290–2300.

Unkles, S.E., Rouch, D.A., Wang, Y., Siddiqi, M.Y., Glass, A.D., and Kinghorn, J.R. (2004). Two perfectly conserved arginine residues are required for substrate binding in a high-affinity nitrate transporter. Proc. Natl. Acad. Sci. USA *101*, 17549–17554.

Unkles, S.E., Karabika, E., Symington, V.F., Cecile, J.L., Rouch, D.A., Akhtar, N., Cromer, B.A., and Kinghorn, J.R. (2012). Alanine scanning mutagenesis of a high-affinity nitrate transporter highlights the requirement for glycine and asparagine residues in the two nitrate signature motifs. Biochem. J. *447*, 35–42.

Wang, Y., Huang, Y., Wang, J., Cheng, C., Huang, W., Lu, P., Xu, Y.N., Wang, P., Yan, N., and Shi, Y. (2009). Structure of the formate transporter FocA reveals a pentameric aquaporin-like channel. Nature *462*, 467–472.

Yin, Y., He, X., Szewczyk, P., Nguyen, T., and Chang, G. (2006). Structure of the multidrug transporter EmrD from Escherichia coli. Science *312*, 741–744.